Development of machine-learned force fields for lithium-manganese-oxide (Li-Mn-O) spinel. Density functional theory accuracy at a lower computational cost

Donald Hlungwani*, *Raesibe Sylvia* Ledwaba, and *Phuti* Ngoepe

Materials Modelling Centre, University of Limpopo, Private Bag x1106, Sovenga 0727, South Africa

Abstract. The on-the-fly machine learning implemented in the VASP code was utilized to generate interatomic potentials for $LiMn_2O_4$ spinel. The potentials will be further expanded to incorporate the Li_2MnO_3 layered character to enable accurate large-scale atomistic simulations of layered-spinel composite structures at practical computational cost. Li_2MnO_3 is incorporated in $LiMn_2O_4$ structures, which are plagued by capacity fading due to the loss of manganese caused by irreversible structural changes, to improve the electrochemical performance of this material. As such, the generated MLFFs in the current study are a significant step in that direction. The MLFFs were able to reproduce the DFT data with a percentage difference of less than 2%, showing impressive accuracy. The generated MLFFs will be further expanded and improved in a future study.

1 Introduction

Manganese-containing cathode materials such as $LiMn_2O_4$ spinel are actively explored as potential replacements for the thermally unstable and costly $LiCoO_2$ lithium-ion batteries (LIBs). This is due to the abundance of manganese and a need to cut the cost of lithium-ion batteries for practical applicability in the emerging sector of electric vehicles [1]. Additionally, $LiMn_2O_4$ spinel possesses a structural framework composed of a cubic close configuration of oxygen ions forming a three-dimensional pathway for lithium ions, which facilitates high-rate capabilities. Additionally, it possesses relatively acceptable thermal stability, and its environmental benignity makes it one of the favourites for revolutionizing LIBs. Currently, a huge percentage of the cost is incurred on the cathode material in comparison to the other components of LIBs [2], and the total energy that can be extracted is largely dependent on the positive electrode as a host of all the lithium ions that are transferred to the anode during operation. The commercialization of $LiMn_2O_4$ spinel is largely delayed by structural changes during operation, which curtails its overall performance. The structural degradation is caused by the self-redox of Mn^{3+} to form Mn^{2+} and Mn^{4+} ($2Mn^{3+} = Mn^{4+} + Mn^{2+}$), uneven distribution of lithium ions in the $[Mn_2O_4]$ frameworks, and the formation of the tetragonal spinel phase driven by the Jahn-Teller effect [3, 4]. Nonetheless, the colossal

* Corresponding author: donald.hlungwani@gmail.com

contribution to the loss of capacity is attributed to the disproportionation reaction and the phase changes powered by the Jahn-Teller effect, which is exacerbated with increasing temperature and voltage. Ren-ji S and colleagues opted for strengthening the M-O framework of spinel by partially substituting Mn with Mg^{2+} to form $LiMn_{1.95}Mg_{0.05}O_4$. A 96.12 % capacity retention was achieved after 100 cycles of the initial discharge capacity of 110.06 mAh/g at 1C [5]. Recently, Chen Y and co-workers synthesized a Zn and Al dual-doped $LiMn_2O_4$ spinel ($LiMn_{1.94}Al_{0.03}Zn_{0.03}O_4$), which delivered an initial discharge capacity of 11.1 mAh/g and returned 90.1% of that capacity after 300 cycles at 1C [6]. The dissolution of manganese in $LiMn_2O_4$ was hindered in a recent study by Yan G. et al. through coating with $MgAl_2O_4$ [7]. The material was stabilized, and the loss of manganese into the electrolyte was also restrained. The $MgAl_2O_4$-coated $LiMn_2O_4$ spinel delivered an initial specific capacity of 120.21 mAh/g and only 5.5 % of it was lost after 100 cycles at 5C [7]. The substantial efforts by various researchers to coat and dope the spinel structure stabilize it and limit the loss of manganese during operation.

However, in both methods the initial discharge capacity is significantly reduced (< 121 mAh/g), and for bulk doping the number of active M ions in the M_2O_4 framework is lowered. In surface doping, the coating layer was found to act as a resistance for ionic and electronic transport, resulting in poor rate capabilities. Nonetheless, researchers also proposed the integration of $LiMn_2O_4$ spinel with lithium-rich Li_2MnO_3 and $LiMnO_2$ layered structures to form a layered-spinel composite, owing to their structural compatibility [8]. In a study by Liu S and co-workers, $LiMn_2O_4$ spinel domains were incorporated in Li_2MnO_3 layered material, which delivered an excellent energy density of 870 W h kg^{-1}. The cathode material was cycled at high voltages (> 5.0 V vs. Li/L^+). and it was able to maintain its capacity during cycling [9]. In such a bifunctional cathode, the spinel component is used to provide high-rate capabilities, and the layered integral is used to tune the manganese oxidation state, contributing enormously to the overall capacity of the material. However, studies of the layered-spinel composites are quite limited both computationally and experimentally. Especially the role of each component on electrochemical, mechanical, and thermodynamic properties, which are essential in the design of high-energy and high-density positive electrode material. A new leaf of computational techniques, such as machine learning, provides new avenues for exploration of material properties and processes at a practical computational cost while provide comparative accuracy to traditional density functional theory (DFT) implementations. In this current study, machine learning is used to capture the potential landscape of $LiMn_2O_4$ spinel from accurate DFT data. Fully optimized $LiMn_2O_4$ containing vacancy and interstitial lattice defects at temperatures between 300 and 600 K was used as training data. The generated potentials are used to find the ground state structure of $LiMn_2O_4$ spinel and its ground state energy. Future work will include the incorporation of Li_2MnO_3 machine learning potentials into the current set to enable the exploration of layered-spinel composite cathode material. The study forms a strong basis for the optimization of the layered and spinel content for designing durable LS composite cathode material with superior electrochemical, mechanical, and thermodynamic properties.

2 Method

In this current study, the potential landscape of lithium-manganese-oxide with a spinel structure crystallizing in the Fd-3m space group is captured by machine-learning techniques implemented in the Vienna Ab initio Simulation Package (VASP). The $LiMn_2O_4$ ground state structures and training data were generated with VASP utilizing the DFT.

2.1 Density functional theory (DFT)

The first principles calculations were carried out with VASP and the selected pseudopotential approximation model as the projector augmented wave (PAW) method to efficiently describe the core and valence electrons [10, 11, 12]. The revised general gradient approximation exchange correlation functional for solids, the PBEsol functional, was chosen for all the DFT calculations performed in this work [13]. PBEsol is a semilocal approximation functional capable of efficiently describing the short-range exchange correlations. Given the widely reported difficulty of DFT in characterizing strong interactions between unpaired electrons in d or f orbitals, we have opted for the DFT+U approach for correct description of the Mn d orbitals. A Hubbard U parameter of 4.0 eV for Mn d orbitals was chosen in line with literature in which it was determined in a self-consistent approach. Moreover, to obtain accurate forces and energies, the cutoff energy for the plane waves is set to 650 eV with a Monkhorst k-mesh of 4x4x4 centered at the Gamma for integration of the Brillouin zone. A 56-atom $LiMn_2O_4$ spinel structure with its symmetry lowered to P1 was fully optimized with a convergence criterion of 0.01 eV/Å for the forces between atoms and 10^{-6} eV/atom for the total energy. Furthermore, the same convergence was used for structure optimization of vacancy and interstitial defective $LiMn_2O_4$ spinel.

2.2 Machine-learning force fields (MLFF)

Machine Learning (ML) as implemented in the VASP [11, 12] is used to characterize the interatomic potentials of $LiMn_2O_4$. The machine learning force fields are generated from accurate forces of interacting atoms and electrons at the DFT level. In order to choose the suitable training data, the learning is carried out on-the-fly during an ab initio molecular dynamics (MD) simulation. In which, upon encounter of a new structure or chemical environment, an ab initio MD is carried out, or the currently generated MLFF is used to perform the MD steps. A probability model is used to determine whether an ab initio MD step is performed or the MLFF is utilized, and this is configured in a way which allows less expensive ab initio steps to be carried out as the MLFF becomes more accurate. The Bayesian linear regression model is utilized to make the determination of the accuracy of the computed forces with the current MLFF owing to its ability to perform fully probabilistic distribution essential for determining the overall uncertainty. In the current study, the potential energy of a system is a parameterized function of local energies of a probability density that defines the distribution of atoms around a given atom. The potential energy function is thus defined as follows:

$$U = \sum_{i=1}^{N_a} U_i,$$

where U denotes the potential energy of a system with Na atoms and U_i. Represents the local energies, which are defined a:

$$U_i = F[\rho_i(\boldsymbol{r})]$$

The local potential energy U_i is a function of the probability density ρ_i of determining the position of another j at an atomic separation distance r around the atom i. The total energy is given by the sum of weighted Gaussians, with coefficients solved by regression. The local environment is represented by descriptors, which are a function of the radial and angular of the surrounding atoms for a chosen atomic site. The radial and angular descriptors are given by the following equations, respectively:

$$\rho_i^{(1)}(r) = \frac{1}{4\pi}\int \rho_i(r\hat{\boldsymbol{r}})d\hat{\boldsymbol{r}}\ ,$$

where the unit vector between the atoms i and j of the vector $\boldsymbol{r}$ is $\hat{\boldsymbol{r}}$.

$$\rho_i^{(2)}(r,s,\theta) = \iint d\hat{\boldsymbol{r}} d\hat{\boldsymbol{s}}\, \delta(\hat{\boldsymbol{r}}.\hat{\boldsymbol{s}} - cos\theta) \sum_{j=1}^{N_a} \sum_{k\neq j}^{N_a} \rho_{ik}(r\hat{\boldsymbol{r}}) \rho_{ij}(s\hat{\boldsymbol{s}})$$

The angle between the two vectors $\boldsymbol{r}_{ij}$ and $\boldsymbol{r}_{ik}$ is denoted by θ and the angular distribution function is given by ρ_i. Moreover, s defines the distances from the ith atom to another atom k. The maximum number of temporary configurations stored as candidates for the training data, ML_MCONF_NEW was set to 5. An ab initio MD calculation was performed when the error of the predicted forces exceeded the ML_CTIFOR threshold of 0.002 eV/atom. The threshold for error estimation is set through the ML_CTIFOR parameter, and the value of 0.002 was found to enforce critical structure learning at the early stages of the training. The value of the ML_CTIFOR is then refined on the fly to promote learning of new atomic environments and to avoid getting stuck on encountered atomic configurations. In order to balance the learning and computational efficiency of the training, the value for ML_SCLC_CTIFOR is set to 0.6.

3 Results and discussion

3.1 On-the-fly machine-learning in the VASP environment

The on-the-fly machine learning implemented in VASP 6.4 was utilized to generate interatomic force fields for the $LiMn_2O_4$ spinel structure [11, 12]. An ab initio MD initial training was carried out under the NPT ensemble at a temperature of 298 K, in which sufficient configurations at this temperature were sampled. The generated MLFF was further expanded by including elevated temperatures (400 K – 600 K) for more atomic environments. Figure 1(a) illustrates the on-the-fly training of the $LiMn_2O_4$ at elevated temperatures, which is continued from an MLFF generated at 298K. The initial starting $LiMn_2O_4$ structure is shown in figure 1(b), containing 8 Li, 16 Mn, and 32 O atoms. In the MD steps between 0 and 3500, the predicted forces between the atoms are less than the Bayesian threshold. This indicates that the starting MLFF was still accurate in the given trajectory, and no computationally expensive ab initio MD steps are carried out in this region. As the MD steps proceed, the error of the predicted forces of the atoms fluctuates, indicating an encounter of new local atomic environments. These new environments are then added to the training set, and a new improved MLFF is generated. The generated atomic configurations to be added to the data set are facilitated by temperature ramping between 400 and 600 K. The choice of adding a new data set to the training data is carried out through the Bayesian linear regression integration in VASP [11, 12]. The Bayesian probability distribution is used as the out-of-sample error, which is the capability of the MLFF in predicting local atomic environments that are outside the training data. As such, a large phase space is then covered, and thus a comprehensive and robust MLFF is generated. Moreover, the in-sample error of the atomic forces is determined by the root mean squared (RMS) error, which determines the average error in the training data. That is how well the generated MLFF is able to reproduce the trained $LiMn_2O_4$ structures obtained in the MD trajectories. In figure 1(a), the RMS error is decreasing as the MD steps and new environments are encountered, indicating that the growth in the training data set facilitates the creation of a sound MLFF.

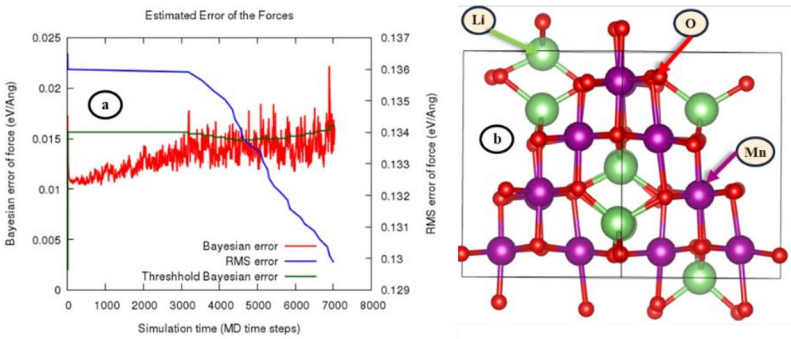

Fig. 1. (a) The Bayesian error and RMS error of the interatomic forces of the MLFF training of (b) the $LiMn_2O_4$ spinel structure from on-the-fly MD data sets created between the temperatures of 400 K and 600 K.

The generated MLFFs in figure 1(a) were further extended by the inclusion of the $LiMn_2O_4$ spinel containing a lithium vacancy illustrated in figure 2(i). This was carried out to incorporate more atomic configurations of the lithium-manganese-oxide spinel atomic configuration phase space to improve the MLFFs. A temperature ramping in the region between 400 and 600 K was carried out to ensure the encounter of new atomic environments during the on-the-fly MD, as shown in figure 2(a). In the MD steps between 0 and 1800, the MLFF-predicted atomic forces are within the set Bayesian threshold, with small fluctuations indicating that the MLFF predictions are not that far off in the current steps. A significant spike is observed around 1900 steps, indicating that an atomic configuration that is far off from the training set has been encountered, and small error spikes are observed between 1900 and 2900 MD steps. As the MD simulation proceeds and the temperature is gradually increased, more and more new local atomic environments are observed, thus improving the training data set and the MLFFs. The RMS error of the atomic forces illustrated in the figure increases in the MD steps between 0 and 2000 and remains constant until 5000 steps. The initial increase of the RMS error is associated with the addition of unique atomic configurations to the current training set due to the introduction of the Li vacancy environment. Furthermore, the predicted RMS errors are less than 1 eV/Å, which is low for the in-sample error. The current MLFF was further improved through the on-the-fly training of Li-vacancy-containing $LiMn_2O_4$ spinel ($Li_6Mn_2O_4$) structures as illustrated in figure 2(b). The $Li_6Mn_2O_4$ spinel structure introduces more Li vacancy environments, which are essential for describing the discharge process. In the MD steps between 0 and 2000, significant spikes of the predicted atomic forces are observed, demonstrating meaningful learning taking place and the addition of new atomic configurations. The predicted errors start to decrease from 2000 MD steps, indicating that the Li-vacancy environments are captured. Furthermore, the in-sample error given by the RMS error is less than 1 eV/Å, indicating good predictive abilities of the generated MLFF for the current training set.

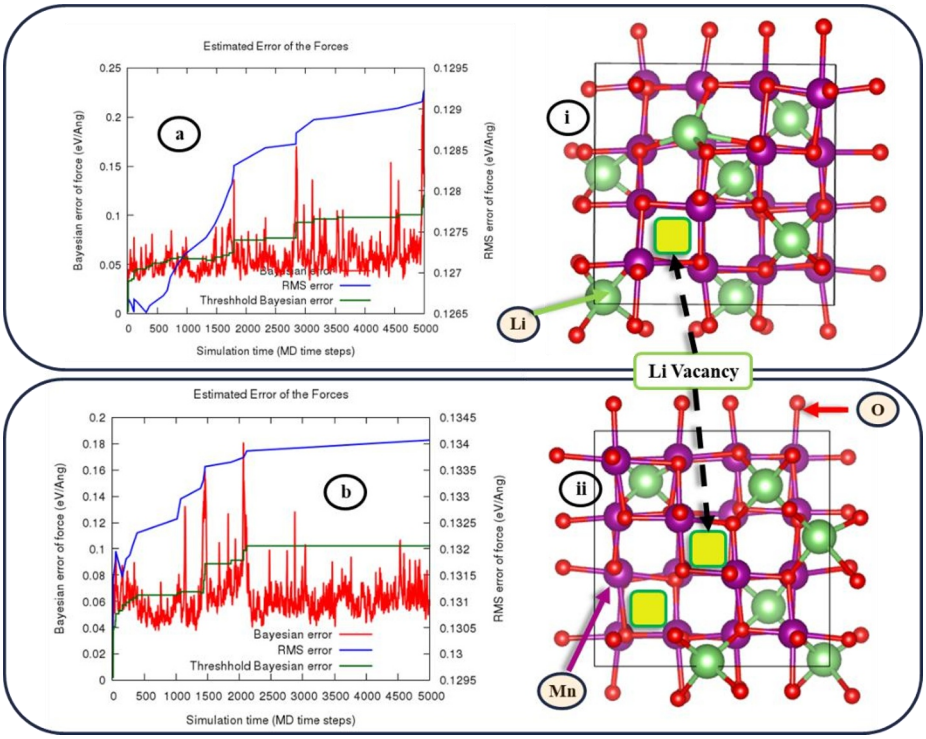

Fig. 2. (a) The Bayesian error and RMS error of the interatomic forces of the MLFF training of (b) $LiMn_2O_4$ spinel structure from on-the-fly MD data sets created between the temperatures of 400 K and 600 K.

3.2 Ground state structure and energy of $LiMn_2O_4$ prediction with MLFFs

Figures 3(a) and (b) show the ground state structure of $LiMn_2O_4$ spinel obtained with the DFT implemented in VASP [11, 12]. The lattice parameters of the VASP-optimized $LiMn_2O_4$ spinel structure are compared with lattice parameters of structures synthesized in experiments. In the current work the DFT cubic lattice parameters of $LiMn_2O_4$ were found to be 8.288 Å, which is comparable to the experimental value of 8.241 Å with a percentage difference of less than 1% [14]. Table 3 shows a comparison between the DFT structure properties and energy calculated with DFT and the generated MLFFs. The generated MLFF reproduces the DFT lattice parameters within a percentage difference of 0.246%. Furthermore, the volume and density of the structure were also reproduced with an acceptable percentage difference of less than 0.734%. The constructed MLFFs were utilized to obtain the ground state energy of the $LiMn_2O_4$ spinel structure, which was found to compare well with the DFT ground state energy within a percentage difference of 1.176%. Therefore, the constructed MLFF is able to describe the potential landscape of $LiMn_2O_4$ and give accurate structural properties and energy of the structure.

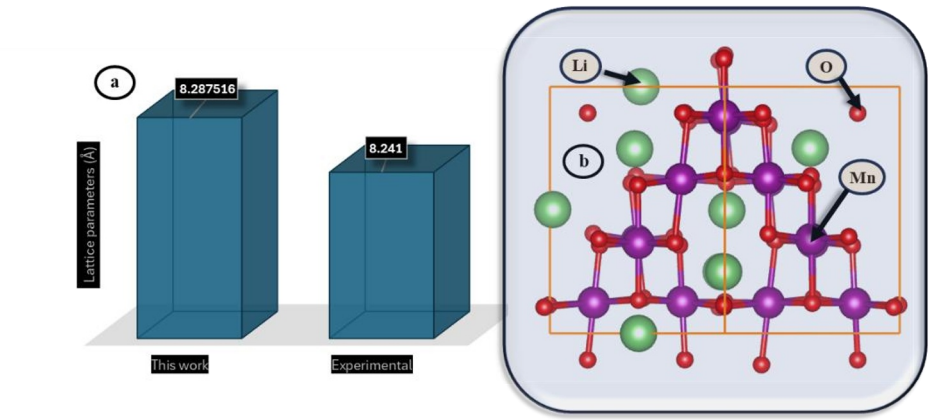

Fig. 3. (a) A bar graph comparing the lattice parameters of (b) the $LiMn_2O_4$ spinel structure calculated in this work and from experimental studies.

Table 1: Comparison of $LiMn_2O_4$ spinel structure parameters calculated with DFT and MLFFs.

Structure property	DFT	MLFF	% Diff (%)
a (Å)	8.288	8.308	**0.246**
b (Å)	8.288	8.308	**0.246**
c (Å)	8.288	8.308	**0.246**
Volume ($Å^{-3}$)	569.211	573.420	**0.737**
Density (Mg/m^3)	4.220	4.189	**0.737**
Total energy (eV)	-50.335	-49.746	**1.176**

4 Conclusion

The potential landscape of the $LiMn_2O_4$ spinel structure was successfully captured with on-the-fly machine learning implemented in VASP [11, 12]. The potentials were utilized to calculate structure properties and ground state energy of the spinel structure. The MLFFs calculated properties compared with a percentage difference of less than 1% to the DFT-calculated properties. In this study, various structures of $LiMn_2O_4$ spinel were used as training data for the generation of MLFFs. The results show that the generated MLFFs can be used to study the $LiMn_2O_4$ spinel structure. Furthermore, the generated MLFFs will be expanded and trained on $LiMn_2O_4$ and Li_2MnO_3 bulk, nanoclusters, and surfaces for studies to enable exploration of layered-spinel composites. In future work, the concentrations of the layered and spinel composites will be optimized to determine the best-performing configuration of the heterostructure to guide in the design of cost-effective, robust, high-energy, and high-power-density lithium-ion batteries.

The authors acknowledge the National Research Foundation (NRF) for financial support and the Centre for High Performance Computing (CHPC). The study is funded by the National Research Foundation (NRF) under the grant reference of PSTD230504101809.

Data will be made available on request.

References

1. S S. Rangarajan, S.P Sunddararaj, A.V. Sudhakar, C.K. Shiva, U. Subramaniam, E.R. Collins, T. Senjyu, Lithium-ion batteries—The crux of electric vehicles with opportunities and challenges. Cleantech. **4**, 908 (2022). https://doi.org/10.3390/cleantechnol4040056
2. Li. Qi, Y. Wang, L. Kong, M. Yi, J. Song, D. Hao, X. Zhou, Z. Zhang, J. Yan, Manufacturing processes and recycling technology of automotive lithium-ion battery: A review. J. Energy Storage. **67**, 107533 (2023). https://doi.org/10.1016/j.est.2023.107533
3. X. Hou, X. Liu, H. Wang, X. Zhang, J. Zhou, M. Wang, Specific countermeasures to intrinsic capacity decline issues and future direction of $LiMn_2O_4$ cathode. Energy Stor. Mater. **57**, 577 (2023). https://doi.org/10.1016/j.ensm.2023.02.015
4. Q. Yu, P. Li, Q. Guo, Synthesis and properties of the $LiMn_2O_4$ cathode material for lithium-ion batteries. Int. Res. J. Pure Appl. Chem. **25**, 14 (2024). https://doi.org/10.9734/irjpac/2024/v25i3852
5. S. Ren-ji, Z. Tong, Z. Yu, X. Xin-yan, W. Tao, M. Zi-yang, T. Pei-yuan, H. Xiang-ping, J. Jian-bing, Doping Mg^{2+} to improve the Li^+ diffusion rate and electrochemical performance of spinel $LiMn_2O_4$. Solid State Ion. **404**, 116434 (2024). https://doi.org/10.1016/j.ssi.2023.116434
6. Y. Chen, M. Li, Q. Zhu, W. Bai, X. Liu, M. Xiang, J. Guo, J. Liu, Enhanced high-rate performance in Zn/Al dual-doped $LiMn_2O_4$ with submicron truncated structure. J. Energy Storage. **82**, 110610 (2024). https://doi.org/10.1016/j.est.2024.110610
7. G. Yan, P. Li, S. Xie, J. Li, W. Li, J. Zheng, M. Yuan, Enhancing structure and cycling stability of $LiMn_2O_4$ cathode materials via $MgAl_2O_4$ surface modification. Ceram. Int. **51**, 12029 (2025). https://doi.org/10.1016/j.ceramint.2025.01.054
8. H. Xie, J. Cui, Z. Yao, X. Ding, Z. Zhang, D. Luo, Z. Lin, Revealing the role of spinel phase on Li-rich layered oxides: A review. Chem. Eng. J. **427**, 131978 (2022). https://doi.org/10.1016/j.cej.2021.131978
9. S. Liu, Y. Wang, D. Xiao, H. Li, T. Wu, B. Wang, G. Hu, L. Wu, Y. Wang, G. Wang, N. Zhang, A highly stable Mn-based cathode with low crystallinity Li_2MnO_3 and spinel functional units for lithium-ion batteries. EES Batteries. **1**, 185 (2025). https://doi.org/10.1039/d4eb00003j
10. G. Kresse, D. Joubert, From ultrasoft pseudopotentials to the projector augmented-wave method. Phys. Rev. B. **59**, 1758 (1999).
11. G. Kresse, J. Hafner, Ab initio molecular-dynamics simulation of the liquid-metal–amorphous-semiconductor transition in germanium. Phys. Rev. B. **49**, 14251 (1994).
12. G. Kresse, J. Furthmüller, Efficiency of ab initio total energy calculations for metals and semiconductors using a plane-wave basis set. Comput. Mater. Sci. **6**, 12 (1996).
13. L.A. Constantin, J.P. Perdew, J.M. Pitarke, Exchange-correlation hole of a generalized gradient approximation for solids and surfaces. Phys. Rev. B. **79**, 075126 (2009). https://doi.org/10.1103/PhysRevB.79.075126
14. H.T. Chung, S.T. Myung, T.H. Cho, J.T. Son, Lattice parameter as a measure of electrochemical properties of $LiMn_2O_4$. J. Power Sources. **97**, 454 (2001). https://doi.org/10.1016/S0378-7753(01)00685-1